

Surface charge effects on the redox switching of LbL self-assembled redox polyelectrolyte multilayers

Mario E. Tagliazucchi, Ernesto J. Calvo *

INQUIMAE, Departamento de Química Inorgánica, Analítica y Química Física, Facultad de Ciencias Exactas y Naturales, Universidad de Buenos Aires, Argentina

Received 25 November 2005; received in revised form 2 February 2006; accepted 6 March 2006
Available online 11 May 2006

Abstract

The effect of surface charge on the electron transfer and charge propagation in layer by layer (LbL) electrostatically self-assembled redox poly-electrolyte multilayers (PEMs) has been studied. Thin films comprised of sequential layers of cationic poly(allylamine) covalently modified by osmium bipyridyl pyridine complexes (PAH-Os) and anionic poly(vinylsulfonate) (PVS) have been studied using electro-chemical impedance spectroscopy (EIS) and ellipsometry. For positively charged topmost layers a transition from low frequency redox pseudocapacitance to diffusion due to electron hopping between adjacent redox sites has been observed. This behavior could be modelled by a bound-diffusion modified Randles electrical equivalent circuit. Negatively charged surfaces terminated in PVS, on the other hand, presented a kinetic hindrance for the osmium redox switching process. This may be ascribed to a limitation in the flux of mobile anions compensating charge due to a skin Donnan potential at the film/electrolyte interface or effects on the local electrostatic environment of the osmium sites. Further adsorption of polycations or charge screening by increasing the electrolyte ionic strength restores the redox charge seen when the polycation was the topmost layer.

© 2006 Elsevier B.V. All rights reserved.

Keywords: Redox polyelectrolyte; EIS; Impedance; Ellipsometry; Osmium bipyridyl; Donnan; Layer by layer; Self-assembled

1. Introduction

In 1992 Royce Murray [1] classified chemically modified electrodes into three categories: (a) monomolecular layers, (b) multimolecular layers and (c) spatially defined, molecularly heterogeneous layers. The latter comprises zeolite and clay modified electrodes as well as multiple layers of redox polymers.

Ion exchange polymers modified electrodes are multimolecular layers films that comprise poly-electrolyte coatings such as Nafion, PVS, PVP, etc. with redox counterions incorporated electrostatically [2]. Donnan equilibrium is observed in this case [3,4]. Unlike ion exchange polymers, LbL electrostatically self-assembled polyelectrolyte multilayers, are reluctant amphoteric

exchangers [5,6] due to intrinsic compensation of polyanion–polyion interactions, resulting in an excess of charge localized at the upper polymer/electrolyte interface and compensated by mobile ions in the solution [7].

Multilayers built by alternated adsorption of anionic and cationic polyelectrolytes allow the synthesis of ultrathin functional films with fine adjustment of film thickness and properties [8,9]. An extension of these PEMs is the introduction of redox ions compensating charge in the otherwise self-compensated or intrinsic PEM, i.e. some polycation–polyanion interaction are exchanged by the redox anion $\text{Fe}(\text{CN})_6^{4-}$ and the redox cation, $\text{Os}(\text{bipy})_3^{3+}$ as studied by cyclic voltammetry and electrochemical impedance spectroscopy [10]. Redox polyelectrolyte multilayers (PEM) self-assembled LbL have been reported with different redox groups attached to polymers: viologen [11–14], ferrocene [15–22], osmium bipyridyl [23–39], sulfonated polyaniline [40], polythiophene [41], cytochrome *c* [42],

* Corresponding author. Tel.: +54 11 4576 3378; fax: +54 11 4576 3341.
E-mail address: calvo@qi.fcen.uba.ar (E.J. Calvo).

myoglobin [43], polyoxo-metalates [44], etc. Hodak et al. introduced in 1997 the use of a ferrocene covalently bound to poly-(allylamine) as a molecular wire to connect electrically the enzyme glucose oxidase in a layer by layer self-assembled (LbL-SA) multilayer to generate an electrical signal in response to molecular recognition of β -D-glucose. Following this first reagentless electrocatalytic active structure based on the successive alternate deposition of ferrocene modified poly(allylamine) cation and anionic glucose oxidase enzyme (GOx), an important number of authors reported similar self-contained redox mediators and enzyme strategy in amperometric biosensors [23–30,33–37,39,45–52].

In PEM structures, the surface potential (ζ -potential) changes alternatively from ca. -50 – 100 mV to 50 – 100 mV when subsequent polyanions or polycations are adsorbed on LbL self-assembled polyelectrolyte multilayers (PEMs) [53–55]. Furthermore, the electrode potential for the oxidation–reduction of redox species in PEMs, measured with respect to an external reference electrode in the electrolyte, also shows an alternating value depending on the charge of the topmost layer [15,17] due to Donnan exclusion of mobile ions carrying the same charge as fixed charges in the thin film PEM [45].

Surface effects with long range consequences have been reported in PEMs. Xie and Granick showed a long-range coupling between ionization groups within weak polyelectrolyte multilayers and charge in the uppermost layer since the whole film responds to a change in surface charge [56]. Schwarz and Schönhoff reported for PAH/PSS PEMs reversible swelling/deswelling driven by the electric potential of the outer layer as positive surface charge leads to film swelling and deswelling occurs for the negatively charged film [55].

In this paper, we study the effects of the surface excess charge on the redox switching: electron transfer and propagation of charge by electron hopping between adjacent redox sites and counter ion mobility, with a combination of EIS and ellipsometry. EIS has extensively been employed to characterize the electrochemistry of redox modified electrodes [57–61]. EIS of LbL self-assembled redox inactive polyelectrolyte multilayers has been reported [10,62,63]; however, to the best knowledge of the authors, this is the first EIS study of a LbL-SA redox polyelectrolyte modified electrode.

2. Experimental section

2.1. Chemicals and solutions

Analytical grade 3-Mercapto-1-propanesulfonic acid sodium salt, MPS (Aldrich), poly(vinyl sulfonic acid, sodium salt), PVS (Aldrich), Poly(allylamine hydrochloride), PAH(Aldrich) were used as supplied. Osmium redox polymer, PAH-Os was synthesized from $\text{Os}(\text{bpy})_2\text{Cl}(\text{py-CHO})\text{Cl}$ complex and freeze-dried PAH as described elsewhere [49]. Aqueous solutions of PAH and PVS 10 mM

(in monomer), were employed for the film preparation by electrostatic adsorption. The osmium redox polymer aqueous solution was dialyzed against water for 3 days before use. The osmium content was evaluated spectrophotometrically at $\lambda = 475$ ($\epsilon = 8,100 \text{ M}^{-1} \text{ cm}^{-1}$). The pH of PAH-Os or PAH polyelectrolyte solutions was adjusted to 8.3 using either HCl or NaOH. A 20 mM MPS solution in 10 mM sulfuric acid (Merck) was freshly prepared in order to avoid oxidation in air. All the solutions were prepared with 18 M Ω Milli-Q (Millipore) deionized water. Other reagents were analytical grade, and they were used without further purification.

2.2. Electrode preparation

Gold coated silicon (100) substrates were employed as electrodes with a 20 nm titanium and 20 nm palladium adhesion layer and a 200 nm gold layer thermally evaporated on silicon with an Edwards Auto 306 vacuum coating system, at $P < 1.10 \times 10^{-5}$ mbar.

In the first step of electrode modification, the freshly evaporated gold film substrates were primed with sulfonate groups by immersion in an MPS solution for 30 min followed by rinsing with deionized water. After thiol adsorption, the first polycation layer was deposited on thiol-modified Au substrate by immersion in PAH-Os solutions for 15 min. The next and subsequent layers were deposited onto the modified surface by alternate immersion for 15 min in a solution of the respective polyanion (PVS) and polycation (PAH or PAH-Os) solution, followed by thoroughly rinsing with Milli-Q water. The adsorption times were determined by ellipsometric transient measurements and QCM [15]. In this manner, LbL supramolecular structures of PVS/PAH and PVS/PAH-Os have been built up by reverting the surface charge of the topmost layer.

2.3. Electrochemical impedance spectroscopy (EIS) measurements

Impedance measurements were performed with a purpose built Teflon cell. The geometrical area of the working electrode exposed to solution was approximately 0.25 cm^2 and was defined by an inert 'o'-ring. Before thiol adsorption the electrode potential was cycled in 2 M sulfuric acid between 0.2 and 1.6 V at 0.1 V s^{-1} to check for surface contamination and electrochemically active areas were calculated from the reduction peak of gold oxide [64]. An Ag/AgCl 3 M KCl reference electrode was employed and all potentials herein are referred to it. A large area platinum gauze was employed as the auxiliary electrode. All electrochemical experiments were carried out in 20 mM M TRIS buffer solutions of pH 7.4 and the ionic strength was adjusted using KNO_3 .

Electrochemical impedance spectra were recorded using a fast-response potentiostat (Jaissle IMP88, Germany) and a frequency response analyzer (FRA, NF Electronic Instruments model S-5720C, Japan) under computer con-

trol and data acquisition via IEEE 486 interface with a purpose written software. The frequency range was 3–10 kHz to 0.1 Hz and the amplitude of oscillation was set to 10 mV. Data analysis was performed with the program ZView® (Scribner Associates, USA).

2.4. Ellipsometric measurements

Ellipsometric Measurements were employed to determine the thickness of the self-assembled multilayer films, using a SENTECH (Berlin, Germany) variable angle rotating-analyzer automatic ellipsometer (vertical type, 2000 FT model) equipped with a 632 nm laser as polarized light source. All measurements were performed at an incidence angle of 70.00°. The gold electrode was horizontally mounted in a Teflon holder and aligned before each experiment. All adsorption steps were carried out avoiding any variations of the electrode position in order to keep the system alignment. Ellipsometric parameters variation lower than the data dispersion for a single measurement (0.01 in Ψ and 0.05 in Δ) was secured in this way.

Ellipsometric angles Ψ and Δ were determined from reflection-induced changes in the state of polarization of linearly polarized light, which are related to the ellipsometric ratio [46,47]:

$$\rho = \tan(\psi) \cdot \exp(\Delta \cdot i) = \frac{r_p}{r_s}$$

where $\tan \Psi$ represents the amplitude change in ρ , Δ is the phase difference change, and r_p and r_s are the complex reflection coefficients for light polarized parallel and perpendicular to the plane of incidence which depend on the structure and optical properties of the system. Ellipsometric parameters (Ψ and Δ) were collected in operator-triggered mode after each adsorption step with the modified electrode surface in contact with TRIS 20 mM-KNO₃ 0.2 M pH 7.4 buffer solution in a SENTECH liquid cell (E-SE400-20) fitted with two glass optical windows positioned for 70.00° with an accuracy of 0.01°. The experimental data were fitted as described elsewhere [46]. The Ψ vs Δ plots are shown in figure 1S and the ellipsometric thickness vs layer number in figure 2S.

3. Theoretical background

Several models have been developed to analyze the electrochemical impedance spectra of redox polymer films. These models have considered further complexities such as the interaction between redox sites [65]; migration effects [66,67]; slow reaction with soluble species [60,68]; non-uniform film thickness [69,70], etc. However the extensions of the simple interfacial electron transfer and diffusion charge propagation model [71,72] have been made at the expense of a less clear physical insight. In the following we shall use a simple EIS model and discuss its scope and limitations.

The model employed consists of the ohmic electrolyte resistance (R_s) in series with an impedance given by the interfacial double layer capacitance (C_{DL}) in parallel to the Faradaic charge transfer resistance (R_{CT}) and a finite diffusion impedance (Z_D) (modified Randles equivalent circuit [73], see inset in Fig. 1a). The bound diffusion impedance is given by [71]:

$$Z_D(\omega) = R_{CT}(k_f + k_b) \cdot \frac{1}{[jD_{app}\omega]^{1/2}} \coth \left(d \left[\frac{j\omega}{D_{app}} \right]^{1/2} \right) \quad (1)$$

where d is the film thickness, D_{app} is the apparent diffusion coefficient of redox charges in the film, ω is the angular frequency and k_f and k_b are the forward and backward rate constants for the interfacial redox process:

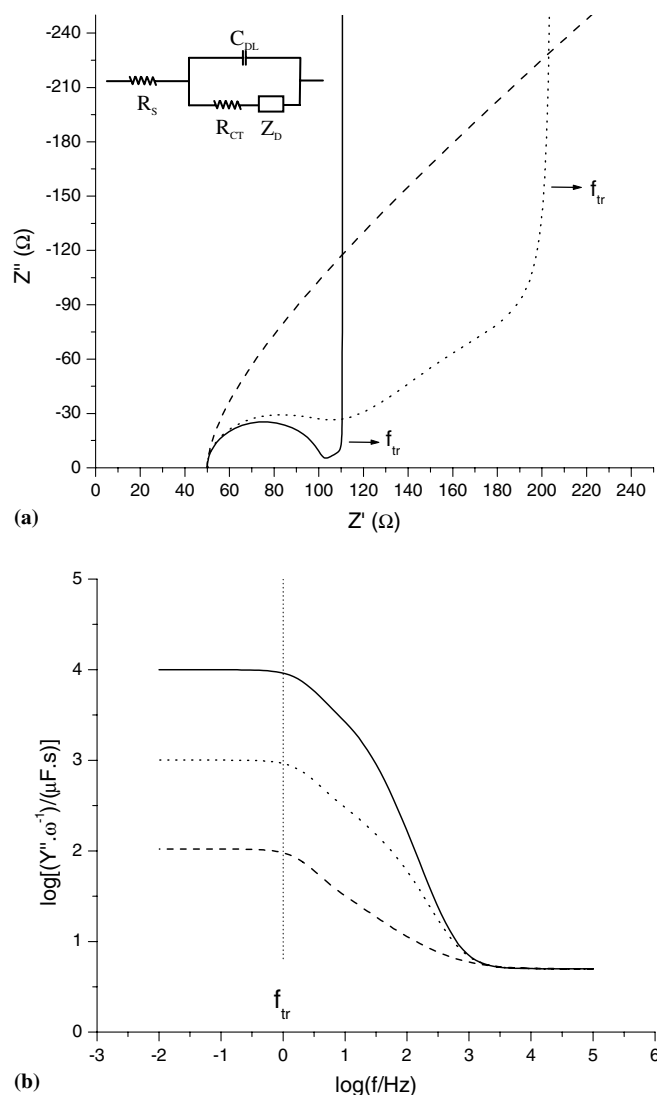


Fig. 1. Ideal Nyquist (a) and $\log(Y''/\omega)$ vs $\log(\omega)$ plot (b) for the circuit shown as an inset. Simulation parameters: R_s : 50 Ω ; R_{CT} : 50 Ω ; C_{DL} : 5 μF ; f_{tr} : 1 Hz. C_F : --- 100 μF , ... 1000 μF and — 10,000 μF respectively. R_s : Solution resistance; C_{DL} : Double layer capacitance at the electrode surface; R_{CT} : Charge transfer resistance; Z_D : Finite diffusional impedance described by Eq. (1).



defined by

$$k_f = k^0 \cdot \exp \left[\frac{\alpha F \eta}{RT} \right] \quad (2b)$$

$$k_b = k^0 \cdot \exp \left[-\frac{(1-\alpha)F\eta}{RT} \right] \quad (2c)$$

where the apparent overpotential, $\eta = E - E_{\text{app}}^0$ is defined with respect to the reference electrode outside the film [45], k^0 is the heterogenous rate constant, F is the Faraday constant and α is the symmetry factor taken as 0.5 for simplicity.

R_{CT} is the charge transfer resistance for the Os(III)/Os(II) reaction:

$$R_{\text{CT}} = \frac{(k_f + k_b) \cdot RT}{C^* \cdot F^2 \cdot A \cdot [k_b k_f]} \quad (3)$$

C^* represents here the total Os volume concentration (mol cm^{-3}) in the film. It is convenient to rewrite Eq. (1) as:

$$Z_D(\omega) = \left[\exp \left(\frac{\eta F}{2RT} \right) + \exp \left(-\frac{\eta F}{2RT} \right) \right]^2 \cdot \frac{RT}{F^2 A C^*} \cdot \frac{1}{[jD_{\text{app}}\omega]^{1/2}} \coth \left(d \left[\frac{j\omega}{D_{\text{app}}} \right]^{1/2} \right) \quad (4)$$

The low and high frequency limits of the impedance and the Faradic capacitance (Y''/ω) are given respectively by:

$\omega \rightarrow 0$

$$Z_D(\omega \rightarrow 0) = \left[\exp \left(\frac{\eta F}{2RT} \right) + \exp \left(-\frac{\eta F}{2RT} \right) \right]^2 \times \frac{RT}{F^2 A C^*} \left[\frac{1}{j\omega d} + \frac{d}{3D_{\text{app}}} \right] \quad (5a)$$

$$Y''/\omega(\omega \rightarrow 0) = - \left[\exp \left(\frac{\eta F}{2RT} \right) + \exp \left(-\frac{\eta F}{2RT} \right) \right]^{-2} \times \frac{F^2 \cdot A \cdot C^* \cdot d}{RT} \quad (5b)$$

$\omega \rightarrow \infty$

$$Z_D(\omega \rightarrow \infty) = \left[\exp \left(\frac{\eta F}{2RT} \right) + \exp \left(-\frac{\eta F}{2RT} \right) \right]^2 \times \frac{RT}{F^2 A C^*} \frac{1}{(j\omega D_{\text{app}})^{1/2}} \quad (6a)$$

$$Y''/\omega(\omega \rightarrow \infty) = - \left[\exp \left(\frac{\eta F}{2RT} \right) + \exp \left(-\frac{\eta F}{2RT} \right) \right]^{-2} \times \frac{F^2 A \cdot D_{\text{app}}^{1/2} \cdot C^* \cdot \omega^{-1/2} \sqrt{2}}{RT} \quad (6b)$$

Inspection of Eqs. (5) and (6) shows in the high frequency limit that the finite diffusion impedance behaves as a semi-infinite Warburg element and in the low frequency limit that the charge propagates reaching the film-electrolyte interface with a pseudo-capacitive behavior. This Faradaic capacitance has a maximum at the E_{app}^0 , given by:

$$C_{\text{F,max}} = \frac{F^2 A \Gamma_{\text{Os}}}{4RT} \quad (7)$$

where Γ_{Os} is the osmium surface concentration (mol cm^{-2}) defined as the product of the film thickness (d) and the volume osmium concentration (C^*).

The potential dependence ($0 \leq f(\eta)^{-1} \leq 1$) is described by

$$f(\eta) = \frac{1}{4} \left[\exp \left(\frac{\eta F}{2RT} \right) + \exp \left(-\frac{\eta F}{2RT} \right) \right]^2 \quad (8)$$

It is convenient to define a characteristic transition angular frequency, ω_{tr} , as

$$\omega_{\text{tr}} = \frac{D_{\text{app}}}{d^2} \quad (9)$$

The transition frequency f_{tr} is equal to $\omega_{\text{tr}}/2\pi$. Combining Eqs. (7)–(9) and re-writing we obtain:

$$Z_W(\omega) = -f(\eta) \cdot \frac{1}{C_F \omega} \left[\frac{\omega}{\omega_{\text{tr}}} \right]^{1/2} \cdot j^{1/2} \cdot \coth \left(\left[\frac{\omega}{\omega_{\text{tr}}} \right]^{1/2} \cdot j^{1/2} \right) \quad (10)$$

$$Y''/\omega(\omega \rightarrow 0) = -\frac{1}{f(\eta)} C_F \quad (11)$$

$$Y''/\omega(\omega \rightarrow \infty) = -\frac{1}{f(\eta)} \sqrt{2} \cdot \left(\frac{\omega}{\omega_{\text{tr}}} \right)^{-\frac{1}{2}} C_F \quad (12)$$

Fig. 1 depicts the expected behavior for Nyquist and $\log(Y''/\omega)$ vs $\log(f)$ plots obtained with Eqs. (10)–(12) and the equivalent circuit in the inset of Fig. 1a using values in accordance with the results discussed below for the present modified electrodes. Plots of $\log(Y''/\omega)$ vs $\log(f)$ are the best choice to visualize the transition from diffusion in the film to redox pseudo-capacitive behavior.

4. Results and discussion

4.1. Dependence on electrode potential

The complex impedance spectra for (PAH-Os)₃(PVS)₃-PAH-Os have been measured at different electrode potentials from 0.1 to 0.4 V in 10 mV potential steps. The low frequency capacitance (Y''/ω) values for self-assembled films with PAH-Os and PVS topmost layers carrying positive and negative surface charge respectively are depicted in Fig. 2. The low frequency capacitance values can be approximated as the sum of C_{DL} and C_F if the charge transfer and charge transport resistances are negligible.

Excellent fit of the experimental data to Eqs. (8)–(12) shows the Nernstian behavior of the Os redox thin layer for both PAH-Os (+) and PVS (−) finished layers. The characteristic fitting parameters are summarized in Table 1 for both PAH-Os (+) and PVS (−) capped films. A common double layer residual capacitance of approximately $12 \mu\text{F cm}^{-2}$ and an almost ideal peak full width at half height (FWHH) of 98–106 mV are observed. The impor-

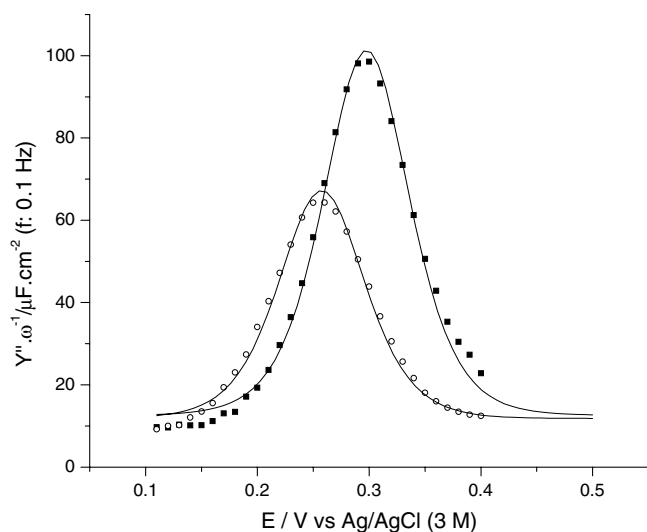


Fig. 2. Low frequency (0.1 Hz) capacitance (Y''/ω) as a function of the electrode potential for (■) (PAH-Os₃/PVS₃)/PAH-Os (+) and (○) PAH-Os₄/PVS₄ (–) electrodes, measured in 20 mM Tris–0.2 M KNO₃ pH 7.4 buffer. Solid lines correspond to fits of the data with Eq. (13) plus a constant to account for the double layer capacitance.

Table 1

Parameters extracted from low-frequency (0.1 Hz) capacitance at different applied potential data (see Fig. 2)

	(PAH-Os) ₄ (PVS) ₃ (+)	(PAH-Os) ₄ (PVS) ₄ (–)
E^0/mV	(298 ± 1)	(258 ± 1)
$C_F/\mu\text{F cm}^{-2}$	(89 ± 2)	(55 ± 1)
$C_{DL}/\mu\text{F cm}^{-2}$	(12.6 ± 0.7)	(11.8 ± 0.5)
$\Gamma_{\text{Os}}/\text{pmol cm}^{-2}$	(94 ± 2)	(59 ± 1)
FWHH/mV	(98 ± 2)	(106 ± 2)

tant difference between similar Os films with positively and negatively charged surface layers is given by the apparent formal redox potential E_{app}^0 and the active redox site concentration i.e. C_F and the surface Os concentration,

$$\Gamma_{\text{Os}} = \frac{4 \cdot R \cdot T \cdot C_{F,\text{max}}}{F^2 \cdot A} \quad (13)$$

respectively.

The difference in apparent redox potential arises from the Donnan potential at the polymer-solution interface as previously described [45], which results from fixed ionic charges in the film which exclude mobile ions of the same charge in the electrolyte from entering into it. An interfacial electrical potential, Donnan potential, balance the difference in the chemical potential of ions in the film and the electrolyte.

The active redox surface concentration of the positively charged surface capped with PAH-Os is more than 60% larger than for the negatively charged film with an extra PVS layer. It should be noted that the number of osmium sites should be the same in both films (same number of PAH-Os layers). This difference is beyond the observed variability for different self-assembled electrodes (10–20%). Similar topmost layer effects on the redox charge

have been described previously with cyclic voltammetry for PAH-Os/PVS, PAH-Os/PSS [45] films, ferrocene-polyallylamine PAH-Fc/GOx [15] and PAH-Fc/PVS [17] films. Three possible explanations have been proposed: (i) desorption of the Os polymer during PVS adsorption (ii) some thermodynamic limitation (iii) or a kinetic hindrance for a fraction of the Os sites to be electrochemically active. Desorption and thermodynamic limitation would imply a smaller amount of accessible redox sites for PVS finished films, irrespective of the experimental time scale. On the other hand, the kinetic hindrance would arise if the redox centers were accessible to electron transfer but the process is too slow with respect to the characteristic time scale in the impedance (ω^{-1}) or the cyclic voltammetry (RT/vF) measurements.

4.2. Dependence on the number of layers

Examination over the whole frequency spectrum for multilayers comprising a different number of PVS and PAH-Os layers can provide evidence of the spatial electrochemically active concentration across the film thickness. The LbL self-assembly technique offers a unique possibility not only to control the topmost surface charge and the film chemical composition but also to produce films with a nanometer scale precision given by the thickness of a single polymer layer. Unlike conventional deposition techniques such as spin coating and electro-polymerization, the LbL self assembly of redox polyelectrolytes allows the effects resulting from composition and surface charge to be distinguished from those due to film thickness.

Fig. 3 shows a $\log(Y''/\omega)$ vs $\log(f)$ plot at different stages of the self-assembly process for a (PAH-Os)₁₂(PVS)₁₂PAH-Os multilayer modified electrode. After each adsorption step, the maximum of the low frequency capacitance (Y''/ω) was determined for the electrode and used to measure the EI spectra at the E_{app}^0 , which varied by the Donnan potential. Comparison of Fig. 3a (even number of adsorption steps) and b (odd number of adsorption steps) shows that the $\log(Y''/\omega)$ vs $\log(f)$ plots are strongly affected by the nature of the topmost layer, i.e. PAH-Os or PVS respectively. For films with PAH-Os (+) as the last adsorbed layer a similar behavior to that described in Fig. 1b is observed. On the other hand, the plots for PVS (–) capped films differ appreciably from the model in Fig. 1b and the measured capacitance is always smaller than that measured before PVS adsorption for the same PAH-Os number of layers in the film (inset Fig. 3b).

In Fig. 3a we observe a shift of the transition frequency ($f_{\text{tr}} = \omega_{\text{tr}}/2\pi$) to lower values as more PAH-Os layers are added as expected from Eq. (9), but for PVS terminated films in Fig. 3b the transition frequency is never reached even at frequencies as low as 0.1 Hz. For these films, at all frequencies the slope of $\log(Y''/\omega)$ vs $\log(f)$ plot is smaller than the value 0.5 expected for a diffusional Warburg impedance, and increases slightly with the number of layers. Comparison with Fig. 3a shows that the limiting low

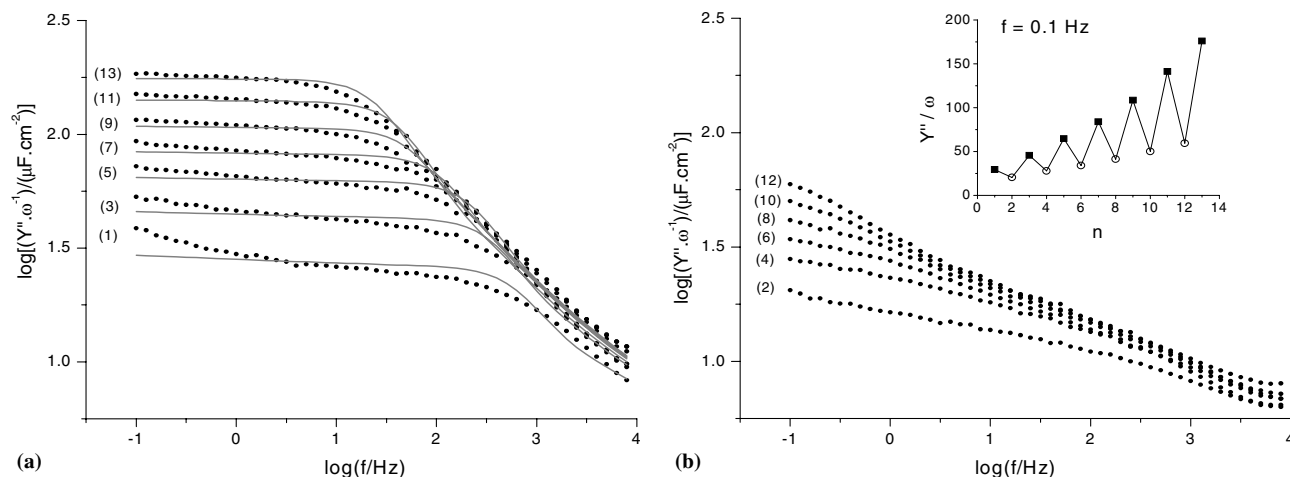


Fig. 3. $\log(Y''/\omega)$ vs $\log(\omega)$ plots for: (a) PAH-Os_m/PVS_n films finished in PAH-Os (+) and (b) PAH-Os_m/PVS_n films finished in PVS (-). The number at the left of each curve is the number of the adsorption steps ($n + m$). All these measurements were made in 20 mM Tris–0.2 M KNO₃ pH 7.4 buffer at the apparent $E_{\text{Os(III)/Os(II)}}^0$. Solid lines in (a) represent the best fits with circuit 1 (see main text). Inset: Y''/ω at 0.1 Hz vs number of layers, n for films finished in (■) PAH-Os and (○) PVS.

frequency capacitance would be eventually reached below 1 mHz, which corresponds to an extremely slow process.

4.3. Effect of electrochemically inactive top layers

Next we shall examine if the blocking effect for charge transport is due to a negative surface charge or the lack of electroactive Os polymer in the topmost layer in contact with the supporting electrolyte. Previous studies carried out by Liu et al. [17] on the self assembled PAH-Fc/PVS have shown that the decrease in redox charge after a PVS layer is assembled on a PAH-Fc capped film could be partially restored by the adsorption of an electroinactive PAH or PDDA layer. Furthermore that report demonstrated that PVS and PAH layers could be assembled in rather thick films where the effect of the capping polyelectrolyte layer was still fully noticeable.

Fig. 4 depicts the results of EIS study on a (PAH-Os)₅(PVS)₅ film when an extra layer of electroinactive but positively charged PAH is adsorbed on top of the redox multilayer. Curve a corresponds to (PAH-Os)₅(PVS)₄ multilayer terminated in PAH-Os, while curve c shows the behavior of (PAH-Os)₅(PVS)₅ with a negatively capping layer as previously shown in Fig. 3. Curve b shows how the redox capacitance of the electrode depicted in curve b increases after adsorbing PAH from the solution, reaching almost the behavior of the electrode terminated in PAH-Os. Thus, the nature of charge in the topmost layer strongly affects the amount of accessible electroactive material in the self-assembled PAH-Os/PVS multilayer.

It should be noted the the number of electroactive Os sites in the film is the same for the cases presented in curves b and c. However, in the time scale of these experiments the extra PAH layer has an important influence increasing the number of osmium redox sites in the film that can be oxidized and reduced.

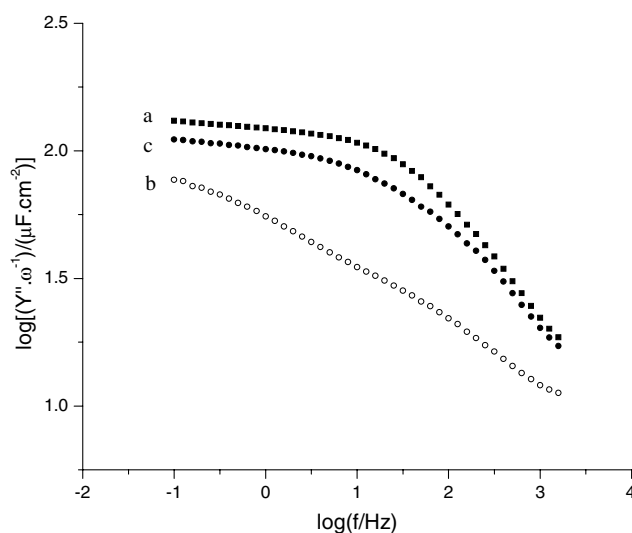


Fig. 4. $\log(Y''/\omega)$ vs $\log(\omega)$ plots for: (a) (PAH-Os₄/PVS₄) PAH-Os (+), (b) PAH-Os₅/PVS₅ (-) and (c) (PAH-Os₅/PVS₅) PAH (+) films in 20 mM Tris–0.2 M KNO₃ pH 7.4 buffer at the apparent $E_{\text{Os(III)/Os(II)}}^0$.

4.4. Effect of electrolyte ionic strength

Fig. 5 shows the electrode capacitance dependence with the electrolyte ionic strength for (PAH-Os)₄(PVS)₄PAH-Os (+) (a) and (PAH-Os)₅(PVS)₅ (-) (b). While the ionic strength does not affect the capacitance curve for the positively charged surface film (Fig. 5a), it has a strong effect on the negatively charged electrode, raising the capacitance as the supporting electrolyte concentration increases up to 1.14 M (Fig. 5b). At such electrolyte concentration, the capacitance becomes independent of the ionic strength and reaches the value of the positively charged surface (solid line).

The nature of the redox charge suppression upon adsorbing a top negative layer and the charge restoration

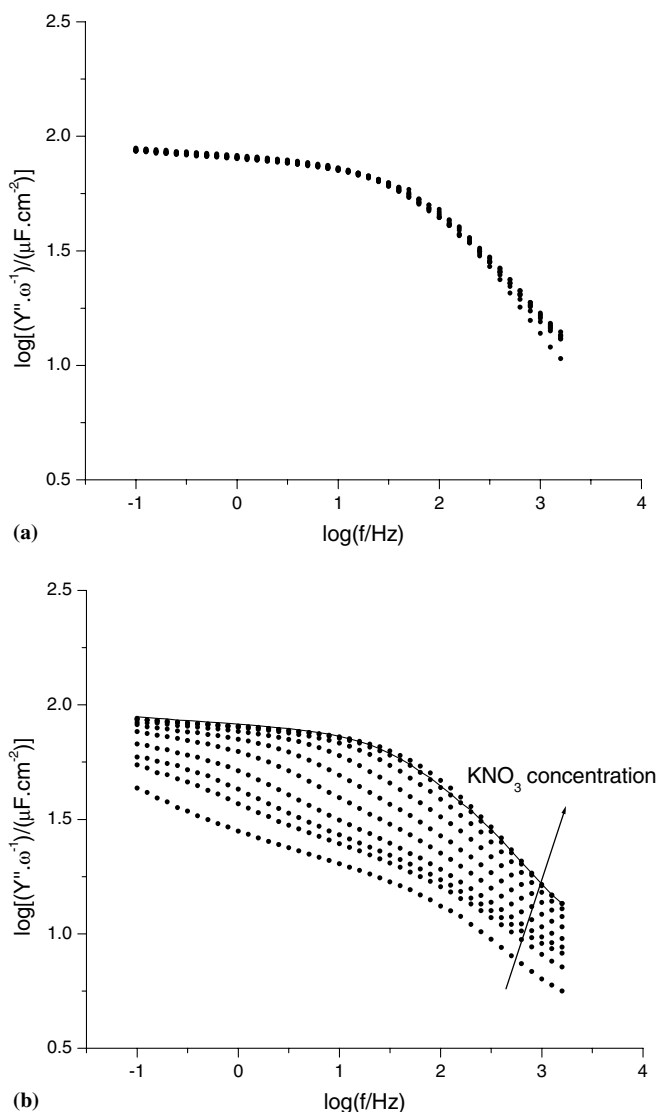


Fig. 5. $\log(Y''/\omega)$ vs $\log(\omega)$ plots for: (a) (PAH-Os₄/PVS₄)/PAH-Os (+) and (b) PAH-Os₅/PVS₅ (–) in Tris 20 mM pH 7.4 buffer solutions of different ionic strengths. KNO₃ concentrations (in mM) were: 27, 82, 134, 200, 310, 520 and 690 for (a) and (from bottom to top): 27, 82, 134, 200, 310, 520, 690, 921, 1140, 1340 and 1500 for (b). Solid line in (b) corresponds to the KNO₃ concentration: 690 mM plot in (a).

by either reverting the topmost layer's positive charge or screening charges by increasing the ionic strength demonstrates the electrostatic nature of the surface effect.

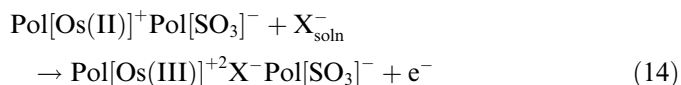
During redox switching of Os(II)/Os(III) in the self-assembled polyelectrolyte multilayer exchange of ions with the supporting solution is necessary in order to maintain the electroneutrality. Probe beam deflection (PBD) studies of PAH-Os/PVS films have shown that the main ion exchange during the oxidation (reduction) of the osmium sites in the film is the ingress (egress) of anions from (to) the external electrolyte [38]. Furthermore, an important conclusion of PBD experiments has been that even the anion exchange is always the major contribution to charge balance, the ratio of exchanged cation to anion is less for negatively charged capping layers. This is also consistent

with the negative slope of the apparent redox potentials with the logarithm of the ionic concentration (Donnan plot) [45].

In nanofiltration membranes built by alternate polyelectrolyte adsorption, electrostatic exclusion is a major factor for ion transport selectivity. Bruening et al. [74] have shown that the rejection flux and selectivity of non redox-active ions can be tailored in PAH/PSS self-assembled membranes by changing the outermost layer charge.

Schlenoff [5] has recently shown that LbL self assembled polyelectrolyte multilayer membranes affect the transport of redox-active probe anions such as hexacyanoferrate (II). While enhanced transport of negative ions through multilayers bearing positive surface charge has been observed, slower rates of ionic transport are apparent for films terminated in layers bearing a negative surface charge. Classical ion exchange membranes exhibit permselective Donnan exclusion of like-charged mobile species, competition of solution ionic species for a number of ion exchanging sites in the membrane results in equilibrium. In the present redox reluctant amphoteric exchangers (term coined by Schlenoff [6]) the additional exchanging sites are created by imbalance of the electrical charge produced by the electrochemical reaction at the underlying metal/polyelectrolyte multilayer interface, i.e. oxidation of Os(II) to Os(III). Another way to create additional exchanging sites is by contact with external ions in the electrolyte as shown by Schlenoff [6] for the transition from intrinsic PEMs with only polyion–polyion electrostatic interactions to polyion–mobile ion interactions. At very high electrolyte concentrations Donnan breakdown is reached and the membrane can exchange electrically neutral species (solvent and ion pairs).

Unlike the transport of mobile redox-active ions through polyelectrolyte membranes [5,6,10] in the present study fixed redox-active ions in the membrane can create charge in excess by an electron hopping mechanism between neighboring sites and a charge transfer reaction at the underlying metal–polyelectrolyte membrane interface (Os(II) → Os(III) + e[−]). The excess charge in the redox polyelectrolyte needs to be balanced by the exchange of redox inactive ions with the liquid electrolyte:



where the Pol[Os] and Pol[SO₃] represent an osmium site in PAH-Os or a sulfonate group in PVS respectively. In Donnan equilibrium, at the film/electrolyte interface the movement of ions across the interface required to maintain electroneutrality is assumed to be rapid. However, the frequency dependence of the electrode capacitance has a distinctive pattern for positively capped or negatively capped LbL multilayer PAH-Os/PVS modified electrodes as shown in Fig. 3a and b. When PAH-Os is the outermost layer of the LbL self assembled multilayer, the capacitance vs logarithm of frequency plots can be described by Eq.

(12) except for a small slope at very low frequencies while Eq. (11) predicts a constant capacitance. This is already known from reported impedance studies of redox active polymer electrodes [69,75]. At low frequency, the redox capacitance increases with the number of LbL polyelectrolyte layers and is almost independent of the frequency since all redox sites in the film are accessible to the propagation of charge from the metal/polyelectrolyte interface. As the frequency of the ac perturbation increases, the capacitance decreases for a given number of LbL layers reaching a common Warburg slope when charge transport becomes the limiting step for the propagation of charge. In this region, the increase of frequency means that the redox perturbation probes less deeper regions of the polyelectrolyte film. In the high frequency limit the electrode-electrolyte double layer capacitance appears as the limiting value.

Inspection of Eqs. (2a), (2b), (3) and (12) indicates that it is possible to obtain quantitative information on the charge transfer coefficients for the Os(II)/Os(III) interfacial reaction and the apparent charge diffusion coefficient that results from electron hopping between suitably positioned osmium sites and movement of ions to compensate the electrical charges [61,66,69].

4.5. Determination of the charge transfer resistance

Electrochemical Impedance Spectra for (PAH-Os)₄(PV-S)₄PAH-Os (+) have been measured at different potentials from 0.1 to 0.4 V with a 10 mV potential step. Some of the resulting Nyquists plots are presented in Fig. 6 as a function of the bias potential. The curve measured approximately at E_{app}^0 for Os(III)/Os(II) couple in the film, ca. 0.30 V, bends downwards earlier than the curves at others

potentials, indicating the lowest value for R_{CT} at this potential. Fitting the whole spectrum to the equivalent circuit in the inset of Fig. 1a yields large errors in the high frequency regions, and thus we have fitted only the high frequency data at 0.3 V (1–10 kHz) with an R-[R-C] circuit [76], which yields $R_{\text{CT}} = 23 \pm 1 \Omega \text{ cm}^2$, $C_{\text{DL}} = 7.5 \pm 1.0 \mu\text{F cm}^{-2}$ and $R_s = 51.4 \pm 1.0 \Omega$. From R_{CT} at $E = E_{\text{app}}^0$, the exchange current density, j_0 and k^0 can be obtained with the following expression:

$$j_0 = Fk^0 C^* = \frac{RT}{FA} \frac{1}{R_{\text{CT}}} \quad (15)$$

for which the redox concentration C^* needs to be known. In the calculation, $C^* = (96 \pm 3) \text{ mM}$ was employed as explained below. The resulting apparent value for k_{app}^0 of $(1.5 \pm 0.1) \times 10^{-4} \text{ cm s}^{-1}$ is very similar to the value of $(3.4 \pm 0.7) \times 10^{-4} \text{ cm s}^{-1}$ observed employing EIS for PSS films containing the Os(bpy)₃^{2+/3+} cation electrostatically bound [61]. These values are about 50–100 times smaller than those observed employing CV for a metallopolymer containing the redox group [Os(N,N'-alkylated-2-2'-biimidazole)₃]^{2+/3+} attached to the polymer by a long aliphatic chain (k_0 : $5\text{--}7 \times 10^{-3} \text{ cm s}^{-1}$) [77] and for the complex cation Os(bpy)₃^{2+/3+} in 0.1 M Na₂SO₄ solution (k_0 : $(1.55 \pm 0.03) \times 10^{-2} \text{ cm s}^{-1}$) [78]. Note that redox groups tethered to polymer modified electrodes have restricted access to the electrode surface as compared to freely diffusing redox species and thus lower apparent k^0 values.

The observed value for the double layer capacitance of $(7.5 \pm 1.0) \mu\text{F cm}^{-2}$ is of the same order of magnitude as those typically obtained for Au/MPS ($7\text{--}10 \mu\text{F cm}^{-2}$) [79]. This is in agreement with previous studies of the systems PAH/PVS and PDDA/PVS where no substantial decrease in the double layer capacitance is observed during the assembly of up to 16 bilayers of these polyelectrolytes on top of Au/MPS [80].

4.6. Determination of redox sites concentration

The redox site concentration was extracted from the low frequency impedance of Z_D as described by Eqs. (7) and (12). The experimental data for PAH-Os capped films was fitted with the equivalent circuit (see inset in Fig. 1a), replacing the C_{DL} with a constant phase element (CPE) [81]:

$$Z_{\text{CPE}} = \frac{1}{Q} \left(\frac{1}{i \cdot \omega} \right)^\gamma$$

where γ is related to the phase and Q is a constant with dimensions of $\text{F s}^{\gamma-1}$. The values used in the fitting procedure, $9.4 (\mu\text{F cm}^{-2}) \text{ s}^{-0.05}$ and 0.95 for Q and γ respectively, were obtained for Au/MPS before the first PAH-Os adsorption and were assumed to be valid for subsequent measurements on the basis of previous experiments on the PAH/PVS system. We chose to perform the fitting in that way because the high frequency data was found to convey little information about the C_{DL} (see above). Curves simulated with the obtained parameters and the

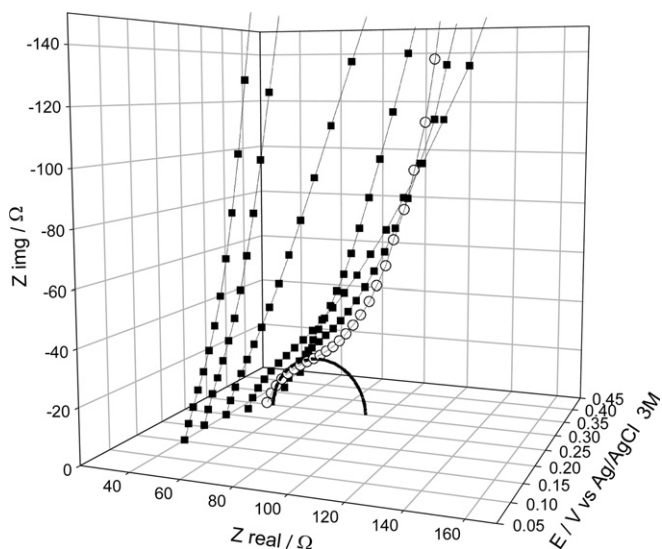


Fig. 6. Nyquist plots for the high frequency part of the EI spectra, measured at different bias potentials for (PAH-Os)₃(PVS)₃/PAH-Os in 20 mM Tris–0.2 M KNO₃ pH 7.4 buffer. Electrode electrochemical active area: 0.447 cm². (○) data measured at the apparent E^0 (0.3 V), (■) data measured at other potentials. Solid line: semicircle fit for a $R_{\text{CT}} - [R_s - C_{\text{DL}}]$ circuit.

equivalent circuit (inset Fig. 1a) are shown as solid lines in Fig. 3a for comparison. Table 2 lists the values for C_F and ω_{tr} . The values obtained for R_{CT} are close to zero but the very large uncertainties observed ($>20\ \Omega$) make them less reliable. We consider that the semicircle determination used above gives a more reliable value for R_{CT} than those obtained fitting the entire EI spectrum where the statistical weight of the high frequency data is smaller. It can be seen from Fig. 4a and Table 2 that the quality of the fitting is low for the first layers, but it improves considerably for thicker films. This could have an origin in an incomplete electrode coverage when only a few layers have been assembled [62,63]. Even though the simplest model was used to fit the data in this first study of the impedance spectra of an LbL-SA electroactive film, the application of advanced impedance models to our multilayer redox films is under study.

In order to determine the redox center surface concentration, the values of C_F should be transformed, by means of Eq. (7), into the surface concentration Γ (see Table 2). Those values were plotted against the ellipsometric thickness of the film (see Supporting information fig. S1 and S2) in Fig. 7. The surface concentration increases linearly with the film thickness indicating that the concentration of Os sites in the film is independent of the number of assembled bilayers (each layer contributes the same amount of osmium redox centers). The value obtained for the osmium concentration from the slope of this plot was $96 \pm 3\ \text{mM}$, higher than those observed for PAH-Os (Self assembled at pH 8.25)/GOx films ($52\ \text{mM}$) [82] which is consistent with the relative size and conformational degrees of freedom for PVS and GOx respectively.

4.7. Charge propagation diffusion coefficient

Fig. 8 shows a plot of the reciprocal of ω_{tr} against the square film thickness (d^2). According to Eq. (9), the slope of this plot yields a diffusion coefficient for charge transport of $(1.45 \pm 0.02) \times 10^{-10}\ \text{cm}^2\ \text{s}^{-1}$. This coefficient should be regarded as a binary apparent diffusion coefficient since at least two different species could be responsible for charge transport inside the film: the Os(II)/Os(III) centers by an electron hopping mechanism and the counter ions. The overall diffusion process is controlled by the slowest step. Mathias et al. [69] showed that in the case when diffusion is ion-limited the high frequency resistance (R_∞) is expected to become infinite at potentials far from

Table 2
Best fit parameters for EIS data of PAH-Os finished layers in Fig. 5a

Layer	$C_{F,\text{max}}$ ($\mu\text{F cm}^{-2}$)	ω_{tr} (Hz)	Γ (pmol cm^{-2})
1	19 ± 15	1300 ± 509	21 ± 16
3	36 ± 14	710 ± 139	38 ± 15
5	55 ± 14	424 ± 53	58 ± 14
7	74 ± 11	214 ± 16	79 ± 12
9	98 ± 8	106 ± 4	10.5 ± 0.8
11	131 ± 8	71 ± 2	14.0 ± 0.8
13	166 ± 8	43 ± 1	17.7 ± 0.9

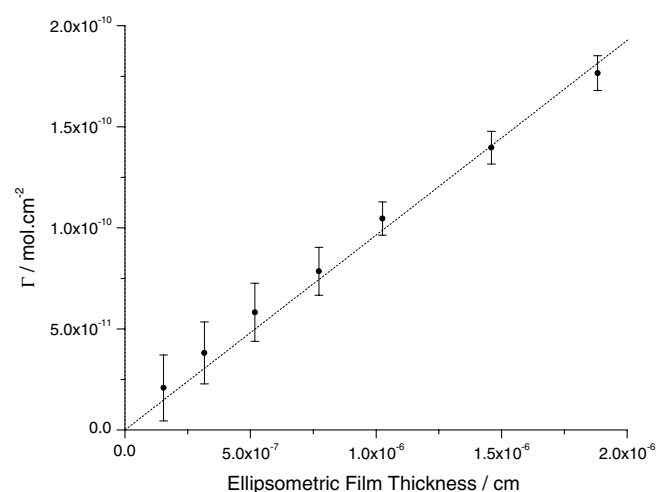


Fig. 7. Γ_{Os} extracted from $C_{F,\text{max}}$ vs ellipsometric thickness for PAH-Os finished films with different number of bilayers. From the fit: C^* : $(96 \pm 3)\ \text{mM}$, R^2 : 0.9985.

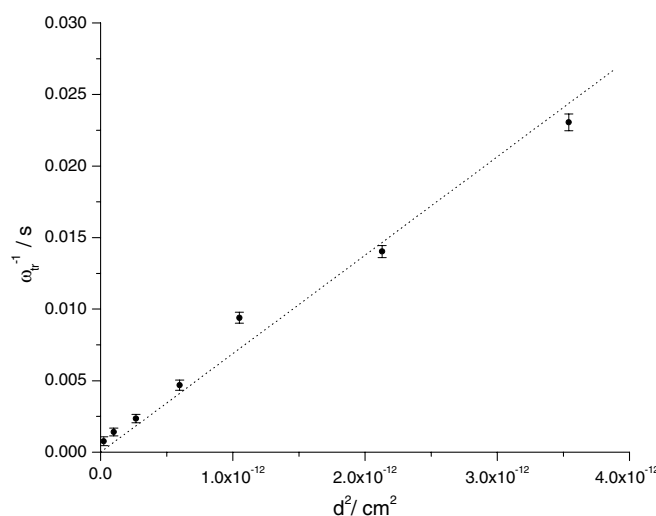


Fig. 8. Plot of ω_{tr}^{-1} vs the square of the ellipsometric thickness employed to determine the apparent diffusion coefficient. From the fit: D : $(1.45 \pm 0.02) \times 10^{-10}\ \text{cm}^2\ \text{s}^{-1}$, R^2 : 0.9871.

$E_{Os(III)/Os(II)}^0$. On the contrary, R_∞ is expected to be potential independent if diffusion is limited by electron hopping. In our case the resistance measured at 10 kHz varies about $2\ \Omega\ \text{cm}^2$ in the potential range 0.1–0.5 V, which means that ion transport is fast and therefore the obtained value for D_{app} is the apparent diffusion coefficient for electron hopping. This result is somewhat expected since it is known that LbL-SA films are permeable to ions due to their high water content [74], and the value agrees with chronoamperometric measurements [83].

5. Conclusions

Layer by layer electrostatically self-assembled redox polyelectrolyte multilayers have been assembled with positively charged PAH-Os and negatively charged PVS. The

use of LbL organized redox films has some advantages over electro-polymerised or spin coated random films such as spatial order, control of thickness in the nanometer scale and control of the surface excess charge of the uppermost layer. This surface charge was regulated by the nature of the terminal capping polyelectrolyte layer alternating positive and negative charges.

The electrochemical redox switching of these modified electrodes was studied by electrochemical impedance spectroscopy, as a function of the number of self-assembled layers, nature of the topmost layer, electrode potential and ionic strength of the supporting electrolyte. The multilayer film thickness was measured by “in situ” ellipsometry and this value was used to calculate the volume concentration of redox centers in the film.

Low frequency capacitance–potential curves show a Nernstian response for a fixed number of redox sites in the surface film and increases with the number of deposited bilayers (PAH-Os/PVS). For positively charged redox films (PAH-Os topmost layer) a model based on electron transfer and bounded diffusion in the film yields the redox charge of the electrode, the diffusion coefficient of electron hopping between adjacent redox sites in the film ($1.45 \times 10^{-10} \text{ cm}^2 \text{ s}^{-1}$), the charge transfer resistance ($23 \Omega \text{ cm}^2$) at the underlying metal–film interface, the double layer capacitance ($7\text{--}10 \mu\text{F cm}^{-2}$) and the uncompensated electrolyte resistance. For negatively capped films (terminated in PVS) a kinetic hindrance for the redox switching becomes apparent: the redox charge obtained from the low frequency capacitance is much less and the frequency dispersion shows a more complex pattern than the corresponding film capped with the polycation.

While the redox capacitance and the concentration of redox charge, which is proportional to its maximum at the formal redox potential, decreases significantly for negatively charged outermost films, partial screening of the excess negative charge at the film/electrolyte interface at higher ionic strength restores the accessibility to the osmium redox sites in the polymer. As $C_{F,\text{max}}$ increases reaching the original value for PAH-Os terminated film at high electrolyte concentrations, breakdown of the Donnan equilibrium occurs [45] and the kinetic hindrance to the flux of anions into the film disappears.

A similar evidence has been observed in cyclic voltammetry where separation of the oxidation and reduction peaks, even at very low scan rates, arises from the electrostatic barrier at the film/electrolyte interface for the ingress and egress of anions during oxidation and reduction of osmium sites in the film respectively [84].

Increasing the ionic strength to reach Donnan breakdown removes the kinetic hindrance which has been associated to a decreased flux of anions that are necessary to balance charge during redox switching. Partial recovery is also obtained upon adsorption of a non-redox polycation (PAH). The kinetic hindrance is of electrostatic nature since it strongly depends on the sign of charge at the topmost layer, and it can be offset by either increasing the ionic

strength thus screening the charges or by adsorbing a positive polyelectrolyte (PAH) as the capping layer reversing the surface charge from negative to positive. In analogy with nanofiltration membranes [74], a possible explanation is a Donnan skin electrostatic effect that would produce a kinetic hindrance to the flux of similarly charged ions which are required to compensate charge during the oxidation of Os(II) within the film. Previous studies support evidence for the exchange of anions as the main contributions to the ionic flux during redox switching of the PAH-Os/PVS modified electrodes [38,45].

An alternative explanation is a change in the electrostatic environment of the osmium sites in the redox PEM when an extra negatively charged layer is adsorbed [56]. Studies are currently in progress to answer these questions.

Acknowledgements

The authors are grateful to CONICET, University of Buenos Aires and ANPCyT for financial support. M.T. acknowledges a cooperative research doctoral fellowship from CONICET and TENARIS Corp.

Appendix A. Supplementary data

Results of ellipsometric thickness determination: Ψ vs Δ plots (figure 1S) and thickness vs layer number plot (figure 2S). Supplementary data associated with this article can be found, in the online version, at [doi:10.1016/j.jelechem.2006.03.014](https://doi.org/10.1016/j.jelechem.2006.03.014).

References

- [1] R.W. Murray, in: R.W. Murray (Ed.), *Molecular Design of Electrode Surfaces*, John-Wiley & Sons, New York, 1992, pp. 1–47.
- [2] N. Oyama, T. Ohsaka, in: R.W. Murray (Ed.), *Molecular Design of Electrode Surfaces*, John-Wiley & Sons, New York, 1992, pp. 333–401.
- [3] R. Naegeli, J. Redepening, F.C. Anson, *J. Phys. Chem.* 20 (1986) 6227.
- [4] P. Ugo, F.C. Anson, *Anal. Chem.* 61 (1989) 1802.
- [5] T.R. Farhat, J.B. Schlenoff, *Langmuir* 17 (2001) 1184–1192.
- [6] T.R. Farhat, J.B. Schlenoff, *J. Am. Chem. Soc.* 125 (2003) 4627–4636.
- [7] J.B. Schlenoff, S.T. Dubas, *Macromolecules* 34 (2001) 592–598.
- [8] G. Decher, *Science* 277 (1997) 1232–1237.
- [9] G. Decher, J.B. Schlenoff, *Multilayer Thin Films: Sequentially Assembly of Nanocomposite Material*, Wiley-VCH, Weinheim, 2002.
- [10] S. Han, B. Lindholm-Sethson, *Electrochim. Acta* 45 (1999) 845–853.
- [11] D. Laurent, J.B. Schlenoff, *Langmuir* 13 (1997) 1552–1557.
- [12] J. Stepp, J.B. Schlenoff, *J. Electrochem. Soc.* 144 (1997) L155–L157.
- [13] N.F. Ferreyra, L. Coche-Guerente, P. Labbe, E.J. Calvo, V.M. Solis, *Langmuir* 19 (1997) 3864.
- [14] G. Zotti, S. Zecchin, B. Vercelli, A. Berlin, S. Grimoldi, R. Bertoncello, L. Milanese, *J. Electroanal. Chem.* 580 (2005) 330–339.
- [15] J. Hodak, R. Etchenique, K. Singhal, P.N. Bartlett, E.J. Calvo, *Langmuir* 13 (1997) 2708–2716.
- [16] S.F. Hou, H.Q.A. Fang, Y. Chen, *Analyt. Lett.* 30 (1997) 1631–1641.
- [17] A. Liu, J. Anzai, *Langmuir* 19 (2003) 4043–4046.
- [18] A. Liu, Y. Kashiwagi, J.I. Anzai, *Electroanalysis* 15 (2003) 1139–1142.

- [19] V. Rosca, I.C. Popescu, *Electrochem. Comm.* 4 (2002) 904–911.
- [20] H.C. Yoon, M.Y. Hong, H.S. Kim, *Anal. Chem.* 72 (2000) 4420–4427.
- [21] H.C. Yoon, H.S. Kim, *Anal. Chem.* 72 (2000) 922–926.
- [22] T. Fushini, A. Oda, H. Ohkita, S. Ito, *Thin Solid Films* 484 (2005) 318–323.
- [23] A. Narvaez, G. Surez, I. Catalin, C. Popescu, I. Katakis, E. Domínguez, *Biosens. Bioelectron.* 15 (2000) 43.
- [24] Y. Sun, J. Sun, X. Zhang, C. Sun, Y. Wang, J. Shen, *Thin Solid Films* 327–329 (1998) 730–733.
- [25] E.J. Calvo, F. Battaglini, C. Danilowicz, A. Wolosiuk, M. Otero, *Faraday Discuss.* 116 (2000) 47–65.
- [26] E. Calvo, R. Etchenique, L. Pietrasanta, A. Wolosiuk, *Anal. Chem.* 73 (2001) 1161.
- [27] E.J. Calvo, E.S. Forzani, M. Otero, *J. Electroanal. Chem.* 231 (2002) 538–539.
- [28] E.J. Calvo, E.S. Forzani, M. Otero, *Anal. Chem.* 74 (2002) 3281–3289.
- [29] E.S. Forzani, M.A. Perez, M.L. Teijelo, E.J. Calvo, *Langmuir* 18 (2002) 4020.
- [30] E.S. Forzani, M.A. Perez, M.L. Teijelo, E.J. Calvo, *Langmuir* 18 (2003) 9867.
- [31] C. Bonazzola, E.J. Calvo, F. Nart, *Langmuir* 19 (2003) 5279.
- [32] N. Tognalli, A. Fainstein, C. Bonazzola, E.J. Calvo, *J. Chem. Phys.* 120 (2004) 1905.
- [33] E.J. Calvo, C. Danilowicz, A. Wolosiuk, *J. Am. Chem. Soc.* 124 (2002) 2452.
- [34] E.J. Calvo, A. Wolosiuk, *Chem. Phys. Chem.* 5 (2004) 235–239.
- [35] E.J. Calvo, A. Wolosiuk, *Chem. Phys. Chem.* 6 (2005) 43–47.
- [36] C. Danilowicz, E. Cortón, F. Battaglini, E.J. Calvo, *Electrochim. Acta* 43 (1998) 3525.
- [37] E.J. Calvo, C.B. Danilowicz, A. Wolosiuk, *Phys. Chem. Chem. Phys.* 7 (2005) 1800–1806.
- [38] D.E. Grumelli, A. Wolosiuk, E. Forzani, G.A. Planes, C. Barbero, E.J. Calvo, *Chem. Comm.* (2003) 3014–3015.
- [39] C. Danilowicz, J.M. Manrique, *Electrochem. Comm.* 1 (1999) 22–25.
- [40] N. Sarkar, M.K. Ram, A. Sarkar, R. Narizzano, S. Paddeu, C. Nicolini, *Nanotechnology* 11 (2000) 30–36.
- [41] J. Lukkari, M. Salomeki, A. Vinikanoja, T. Caritalo, J. Paukkunen, N. Kochanova, J. Kankare, *J. Am. Chem. Soc.* 123 (2001) 6083.
- [42] M.K. Beissenhitz, F.W. Scheller, W.F.M. Stöcklein, D.G. Kurth, H. Möhwald, F. Lisdat, *Angew. Chem. Int. Ed.* 43 (2004) 4357–4360.
- [43] J.F. Rusling, in: Y. Lvov, H. Möhwald (Eds.), *Protein Architecture*, Marcel Dekker, 2000, pp. 337–354.
- [44] L. Cheng, L. Niu, J. Gong, S. Dong, *Chem. Mater.* 11 (1999) 1465–1475.
- [45] E.J. Calvo, A. Wolosiuk, *J. Am. Chem. Soc.* 124 (2002) 8490–8497.
- [46] E.S. Forzani, M. Otero, M.A. Perez, M.L. Teijelo, E.J. Calvo, *Langmuir* 18 (2002) 4020–4029.
- [47] E.S. Forzani, M.A. Perez, M.L. Teijelo, E.J. Calvo, *Langmuir* 18 (2002) 9867–9873.
- [48] E.S. Forzani, V.M. Solis, E.J. Calvo, *Anal. Chem.* 72 (2000) 5300–5307.
- [49] C. Danilowicz, E. Corton, F. Battaglini, *J. Electroanal. Chem.* 445 (1998) 89.
- [50] Y. Sun, J. Sun, Z. Wang, C. Sun, Y. Wang, X. Zhang, J. Shen, *Macromolecular Chemistry and Physics* 202 (2001) 111–116.
- [51] J.S.Y. Sun, X. Zhang, C. Sun, Y. Wang, J. Shen, *Thin Solid Films* 327–329 (1998) 730–733.
- [52] Z.W.W. Li, C. Sun, M. Xian, M. Zhao, *Analytica Chimica Acta* 418 (2000) 225–232.
- [53] F. Caruso, H. Lichtenfeld, E. Donath, H. Möhwald, *Macromolecules* 32 (1999) 2317–2328.
- [54] G. Ladam, P. Schaaf, J.C. Voegel, P. Schaaf, G. Decher, F. Cuisinier, *Langmuir* 16 (2000) 1249–1255.
- [55] B. Schwarz, M. Schönhoff, *Langmuir* 18 (2002) 2964–2966.
- [56] A.F. Xie, S. Granick, *J. Am. Chem. Soc.* 123 (2001) 3175–3176.
- [57] C.R. Martin, I. Rubinstein, A.J. Bard, *J. Am. Chem. Soc.* 104 (1982) 4817–4824.
- [58] H.S. White, J. Leddy, A.J. Bard, *J. Am. Chem. Soc.* 104 (1982) 4811–4817.
- [59] G. Láng, J. Bácskai, G. Inzelt, *Electrochim. Acta* 38 (1990) 773–778.
- [60] C. Bonazzola, E.J. Calvo, *J. Electroanal. Chem.* 449 (1998) 111–119.
- [61] M. Sharp, S. Åberg, *J. Electroanal. Chem.* 449 (1998) 137–151.
- [62] T.H. Silva, V. Garcia-Morales, C. Moura, J.A. Manzanares, F. Silva, *Langmuir* 21 (2005) 7461–7467.
- [63] S.V.P. Barreira, V. García-Morales, C.M. Pereira, J.A. Manzanares, F. Silva, *J. Phys. Chem. B* 108 (2004) 17973–17982.
- [64] H.O. Finklea, D.A. Snider, J. Fedyk, *Langmuir* 6 (1990) 371.
- [65] R.D. Armstrong, B. Lindholm, M. Sharp, *J. Electroanal. Chem.* 235 (1987) 169.
- [66] M.F. Mathias, O. Haas, *J. Phys. Chem.* 96 (1992) 3174.
- [67] R.P. Buck, C. Mundt, *Electrochimica Acta* 44 (1999) 2105.
- [68] G. Láng, G. Bácskai, G. Inzelt, *Electrochim. Acta* 38 (1991) 773.
- [69] M.F. Mathias, O. Haas, *J. Phys. Chem.* 97 (1993) 9217–9225.
- [70] G. Láng, G. Inzelt, *Electrochim. Acta* 36 (1991) 847.
- [71] C. Gabrielli, O. Haas, H. Takenouti, *J. Appl. Electrochem.* 17 (1987) 82–90.
- [72] R.D. Armstrong, *J. Electroanal. Chem.* 198 (1986) 177–180.
- [73] J.E.B. Randles, *Discussions of the Faraday Society* 1 (1947) 11.
- [74] J.J. Harris, J.L. Stair, M.L. Bruening, *Chem. Mater.* 12 (2000) 1941–1946.
- [75] M. Ujvári, G. Láng, G. Inzelt, *Electrochem. Commun.* 2 (2000) 497–502.
- [76] A.J. Bard, L.R. Faulkner, *Electrochemical Methods*, second ed., New York, John Wiley and Sons, 2001.
- [77] R.J. Forster, D.A. Walsh, N. Mano, F. Mao, A. Heller, *Langmuir* 20 (2004) 862–868.
- [78] J.J. O’Dea, J.G. Osteryoung, T. Lane, *J. Phys. Chem.* 90 (1986) 2761.
- [79] C. Mokrani, J. Fatisson, L. Guérente, P. Labbe, *Langmuir* 21 (2005) 4400–4409.
- [80] M. Tagliazucchi, E.J. Calvo, unpublished results.
- [81] G.J. Brug, A.L.G.V.D. Eeden, M. Sluyters-Rehbach, J.H. Sluyters, *J. Electroanal. Chem.* 176 (1984) 275–295.
- [82] V. Flexer, E.S. Forzani, S. Ludueña, L. Pietrasanta, E.J. Calvo, *Anal. Chem.* 78 (2006) 399–407.
- [83] M. Tagliazucchi, D. Grumelli, C. Bonazzola, E.J. Calvo, *Journal of Nanoscience and Nanotechnology*, in press.
- [84] M. Tagliazucchi, P. Bartlett, E.J. Calvo, in preparation.